A Method of Constraint Handling for Speed-Controlled Induction Machines

Zheng Hu and Kay Hameyer, *Senior Member, IEEE*

***Abstract*—This paper focuses on the constraint handling for induction machines (IMs) using model predictive control (MPC) to enhance the optimality. Commonly, the constraints of IMs are represented by stator current and voltage limits, which are described as quadratic inequality in *dq*-frame. Due to the spherical feature, the constraints have to be replaced by approximation by polygon in order to get a standard form of quadratic programming (QP). In this paper, a novel approach is proposed to convert the quadratic inequalities into linear ones without approximation, whereat the inequality is parameter-varying. To tackle this parameter-varying inequality, the multiparametric quadratic program (mp-QP) algorithm for reference tracking is utilized and extended. To ensure the optimization problem solved in real time, an explicit MPC (EMPC) via mp-QP is applied instead of any online numerical solver.**

***Index Terms*—Constraint handling, induction motor control, model predictive control (MPC), offline optimization.**

I. Introduction

THE induction machine (IM) is widely used in electric drive systems because of its simple and reliable structure, low material, and manufacturing cost. To obtain high-performed torque, speed, or position control, the vector control [1], also called field-oriented control (FOC), was developed for practical usage of ac machines since the 1980s and represents nowadays the state of the art. In most cases, the requirements of drive applications can be met by dint of field-oriented cascaded PI controllers. However, for highly dynamic drive applications such as electric drive systems, the cascaded PI controllers are no longer suitable, as the small time constants of inner control loops are added and the system dynamic is thereby deteriorated [2]. With the development of microcontroller techniques in the last few decades, the model predictive control (MPC) is increasingly discussed and proposed for electric drives [3].

MPC originated in late seventies [4] and has been developed intensively in the last three decades [5], [6]. It became one of the most important advances in the processing industry. In 1978, Richalet *et al.* presented "model predictive heuristic control" [7], and in 1979, Culter and Ramaker applied dynamic matrix control (DMC) to a fluid catalytic cracker [8]. In 1980s, MPC became more popular in chemical-process industries, especially in the petrochemical sector [9]. In comparison to PI controller, MPC shows strong abilities to cope systematically with multivariable systems, uncertainties, and constraints [4]. The system constraints can be incorporated into the control objective function, which usually is able to be formulated as a quadratic programming (QP) problem. In [10]–[16], the stability and the optimality of constrained MPC are discussed. In IM, the system constraints are given by maximum admissible stator current which is dependent on the thermal classification of the motor's insulation system, and maximum available dc-link voltage of the inverter, which have to be considered for safety reason in the control strategy. However, the stator current and voltage limits, without consideration of overmodulation by means of space-vector modulation (SVM), are represented in *dq*-frame circularly, which means that the constraints are depicted by quadratic inequalities. They do not fulfill the standard form of QP anymore and therefore have to be rearranged.

The simplest way of constraint handling for IM is to define the limiting values as constants. In [17], three box-constrained inequalities are given, respectively, for *d*-current, torque, and rotor flux. In [18]–[22], the constraint of *q*-current is formulated assuming that *d*-current is constant. The problem of such an approach is that the feasible regions of the system are not comprehensively taken into account, so that the optimality cannot be guaranteed, or the optimal control is only suitable for a particular operating area. In [23], a penalty of stator current is introduced in the cost function to prevent over current. It is only applicable for the finite-set direct control based on enumeration, since there are finite combinations of control values. In case of optimal control problems with continuous control variables, the optimality will be deteriorated. Another approach is to convert the spherical constraint curves into polygons by approximation [24]. The quadratic inequality can thereby be replaced by a set of linear inequalities. In [25] and [26], the current constraint is defined by an adjustable inequality regarding the actual value of *d*-current and the reference value of *q*-current. The voltage constraint is depicted by a polygon of radius of dc-link voltage of the inverter. However, the accuracy of approximation is strongly dependent on the degree of the polygon. Therefore, a tradeoff between approximation accuracy and computational cost should be considered during controller design.

In this paper, the dependency of maximum admissible stator current and voltage on the torque will be analyzed. The quadratic inequalities of current and voltage can be represented by the linear one of torque. In this way, all feasible regions are covered without approximation for the optimal control.

Manuscript received July 29, 2015; revised October 12, 2015, December 11, 2015, and January 7, 2016; accepted January 23, 2016. Date of publication February 23, 2016; date of current version June 9, 2016.

The authors are with the Institute of Electrical Machines, RWTH Aachen University, 52062 Aachen, Germany (e-mail: zheng.hu@iem.rwth-aachen.de; post@iem.rwth-aachen.de).

Digital Object Identifier 10.1109/TIE.2016.2532843

However, the limited torque depends nonlinearly on the rotor speed, which still has to be tackled.

In online optimization, the parameter-varying limit is calculated in each step. Thereby, the proposed optimization problem can be described as standard QP. There are a lot of numerical methods to solve QP. Reference [27] proposes the interior-point method to MPC. Reference [28] gives an overview of algorithms based on this method. In [4], algorithms based on active-set method for QP are introduced. In [29], a comparison of these two methods for MPC is given. In [30] and [31], the optimization methods are fully delineated. Reference [32] explains systematically efficient solutions while numerically solving convex optimization problems. On purpose of using constrained MPC widely in diverse systems, various algorithms of numerical real-time solution are pursued [33]–[36]. However, numerical online optimization still cannot satisfy the real-time requirement in the applications of high dynamic systems such as electric drives, in which the sampling frequency can be over 10 kHz. In [37], an explicit solution of constrained MPC using multiparametric quadratic program (mp-QP) is introduced. With this concept, the optimization problem can be solved offline, and the controller is able to be depicted by piecewise affine (PWA) functions [38]. By means of efficient search algorithm, the online computation time of optimal control action can be reduced to several microseconds. In [39], an efficient approach for constrained optimal control using mp-QP is developed. Reference [40] gives a review of the main approaches to solve explicit MPC (EMPC) problems via mp-QP.

In order to deal with our aforementioned parameter-varying linear inequality, the mp-QP algorithm is utilized in this paper in such a way that the torque limit is appended as an additional state variable to the parameter vector.

This paper is organized as follows. In Section II, the theoretical background of constrained MPC is given. To attain a standard QP form without approximation, the control-specific quadratic inequality constraints on stator current and voltage are converted to linear parameter-varying inequality on torque. To deal with the proposed optimization problem, the EMPC is introduced in Section III. Based on the mp-QP for reference tracking, the controller is designed. In Sections IV and V, the simulation and experimental results are presented, respectively.

II. Constrained MPC

In this section, the MPC in consideration of system constraints is introduced. In order to get the optimal control action, a standard QP with inequality constraints has to be formulated ultimately.

A. Model Predictive Control

For introduction, the discrete-time linear time-invariant unconstrained system without dead time in the simplified form is considered at first

$$\begin{cases} \boldsymbol{x}_{t+1} = A\boldsymbol{x}_t + B\boldsymbol{u}_t \\ \boldsymbol{y}_t \quad\;\; = C\boldsymbol{x}_t \end{cases} \tag{1}$$

where $\boldsymbol{x}_t, \boldsymbol{x}_{t+1} \in \Re^n$, $\boldsymbol{u}_t \in \Re^m$, and $\boldsymbol{y}_t \in \Re^p$ are, respectively, the state, input, and output vectors of the system. Regarding to different MPC algorithms, various cost functions are proposed. For the purpose of speed control (reference tracking), the cost function of MPC for reference tracking is defined by a quadratic function

$$J = \sum_{k=1}^{N_p} \Bigg[(\boldsymbol{w}_{t+k} - \hat{\boldsymbol{y}}_{t+k})^T Q (\boldsymbol{w}_{t+k} - \hat{\boldsymbol{y}}_{t+k}) + \sum_{k=0}^{N_u-1} \boldsymbol{u}_{t+k}^T R \boldsymbol{u}_{t+k} \Bigg] \tag{2}$$

where N_p and N_u represent the prediction and control horizon length, respectively. $\boldsymbol{w}_{t+k}$, $\hat{\boldsymbol{y}}_{t+k}$, and $\boldsymbol{u}_{t+k}$ are the reference, predicted output, and control vectors at time $t+k$, where $\boldsymbol{u}_{t+k} = \boldsymbol{u}_{N_u-1}$ for $N_u \le k < N_p$. Q, R are symmetric positive definite weighting matrices, which penalize the tracking offset and control value. The control law is computed by minimizing this cost function in each time step.

From (1), the predictions in next N_p steps at time t are computed

$$\boldsymbol{Y} = \begin{bmatrix} CA \\ CA^2 \\ \vdots \\ CA^{N_p} \end{bmatrix} \hat{\boldsymbol{x}}_t + \begin{bmatrix} CB & \dots & 0 \\ CAB & \dots & 0 \\ \vdots & \ddots & \vdots \\ CA^{N_p-1}B & \dots & CA^{N_p-N_u+1}B \end{bmatrix} \boldsymbol{U} \tag{3}$$

where the column vectors $\boldsymbol{Y} \triangleq [\hat{\boldsymbol{y}}_{t+1}^T \; \dots \; \hat{\boldsymbol{y}}_{t+N_p}^T]^T \in \Re^h$ and $U \triangleq [\boldsymbol{u}_t^T \; \dots \; \boldsymbol{u}_{t+N_u-1}^T]^T \in \Re^l$ with $h \triangleq pN_p$ and $l \triangleq mN_u$. By means of vector form, (3) can be expressed as

$$\boldsymbol{Y} = \Psi \hat{\boldsymbol{x}}_t + \Theta \boldsymbol{U}. \tag{4}$$

Substituting (4) into (2), the cost function (2) is rearranged to

$$J = (\boldsymbol{W} - \Psi \hat{\boldsymbol{x}}_t)^T Q (\boldsymbol{W} - \Psi \hat{\boldsymbol{x}}_t) - 2\boldsymbol{U}^T \Theta^T Q (\boldsymbol{W} - \Psi \hat{\boldsymbol{x}}_t) + \boldsymbol{U}^T (\Theta^T Q \Theta + R) \boldsymbol{U} \tag{5}$$

where $\boldsymbol{W} \triangleq [\boldsymbol{w}_{t+1}^T \; \dots \; \boldsymbol{w}_{t+N_p}^T]^T \in \Re^h$. Independent on the case, whether $\hat{\boldsymbol{x}}_t$ is corrected by the observer, this value is known at time step t. Therefore, the only unknown variable of the cost function at time step t is $\boldsymbol{U}$. If there is no constraint, an analytical solution exists providing the optimum as

$$\begin{cases} \frac{\partial J}{\partial \boldsymbol{U}} \stackrel{!}{=} 0 \\ \boldsymbol{U}^* = (\Theta^T Q \Theta + R)^T \Theta^T Q (\boldsymbol{W} - \Psi \hat{\boldsymbol{x}}_t). \end{cases} \tag{6}$$

Thus, the optimum control action in the next time step by utilization of the first element of U^* is defined as

$$\boldsymbol{u}_t = \boldsymbol{u}_t^* \tag{7}$$

which is applied as input to system (1), while the resting part of the control actions is discarded. At the next time step $t+1$, the optimization (6) is shifted one step ahead and the whole procedure is repeated with updated information. Therefore, MPC is also called receding horizon control (RHC).

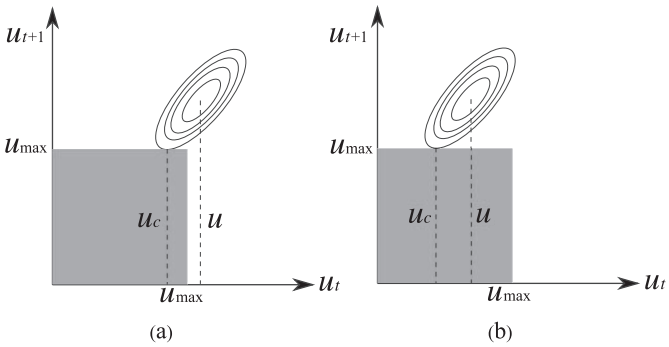

Fig. 1. Computation of control signals with and without incorporation of constraints [4].

B. Quadratic Programming

Almost all real-world physical systems have their constraints, whether they are input, output, or state limits. As mentioned in Section I, one advantage of MPC compared with PI controllers is the incorporation of the system constraints into control design. Hence, MPC provides a good instrument to handle constrained system controlling.

In PI controllers, the system constraints are considered by saturation of the corresponding values and antiwindup in case of actuating value saturation to suppress output overshooting. However, saturation is not a good way for MPC, which will be clarified as follows.

Fig. 1 illustrates the difference between saturation and constraint consideration in MPC. To give a direct insight to the expression, the MPC problem is defined with a control horizon of two. The annular curves represent the values of cost function J. Fig. 1(a) shows the case, in which $\boldsymbol{u}_t$, $\boldsymbol{u}_{t+1} > \boldsymbol{u}_{\max}$. By means of saturation, $\boldsymbol{u}_t$ is forced to its limiting value $\boldsymbol{u}_{\max}$, while by constraint consideration, $\boldsymbol{u}_c$ is applied to reach the minimum of J. In the case of Fig. 1(b), the value of the next control action $\boldsymbol{u}_t$ does not violate the constraint and is therefore applied as input to the system when saturation is executed. In such a way, the cost function value deviates from the optimum solution under constraint consideration, in which u_c is applied to the system.

The example shown in Fig. 1 gives a good explanation, why constraints should be taken into account in MPC design. Now return to the unconstrained optimization problem of MPC. Minimizing the cost function described in (5) is equivalent to the following problem:

$$\min_{\boldsymbol{U}} J' = \frac{1}{2}\boldsymbol{U}^T H \boldsymbol{U} + c^T \boldsymbol{U} \tag{8}$$

where $H = \Theta^T Q \Theta + R$ and $c = -\Theta^T Q(\boldsymbol{W} - \Psi \hat{\boldsymbol{x}}_t)$. It is easily obtained that the Hessian matrix H is symmetric positive semidefinite. Thereby, the optimization problem is specified to a convex optimization, which is illustrated in Fig. 2. The control horizon is set by two steps. In this example, there exists a unique globally optimum solution.

The optimization problem of MPC (8) under consideration of constraints is then depicted as follows:

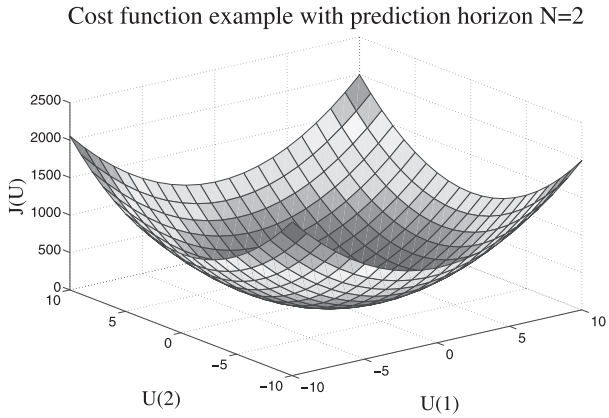

Fig. 2. QP as convex optimization problem.

$$\min_{\boldsymbol{U}} \left\{ \frac{1}{2}\boldsymbol{U}^T H \boldsymbol{U} + c^T \boldsymbol{U} \right\}$$
$$\text{s.t. } G\boldsymbol{U} \leq b + E\hat{\boldsymbol{x}}_t \tag{9}$$

where the vectors $\boldsymbol{G}$, $\boldsymbol{b}$, and $\boldsymbol{E}$ depend on the constraint formulation. For constant constraints, E is equal to zero. Since the box-constraint can be converted to one-sided form, this form is generally valid for all inequality constraint descriptions. Therefore, the optimization problem with constraints is a standard QP. Since the problem is dependent on the state variable $\hat{\boldsymbol{x}}_t$ at each time step, an online solution is required for MPC.

Commonly, the QP problems are solved by efficient numerical solvers based on active-set methods or interior-point methods. With active-set methods, only the active constraints are considered at each iteration step, whereat the active set varies slightly from step to step considering efficiency. However, the active-set algorithms may become slower near to the optimum point. With interior-point or primal dual (PD) interior-point methods, the QP is converted to a Lagrange function with Lagrange multipliers. The constraints are replaced by barrier functions. By means of Karush–Kuhn–Tucker (KKT) conditions [32], the system is converted to nonlinear equations; therefore, at each iteration, the system is linear. Thus, the computation can be accomplished by iterative linear algebraic solvers. The PD interior-point methods feature fast convergence properties. However, the online computational effort for optimal control action is tremendous despite of the efficient numerical solvers. In Section II-C, the approach proposed in [37] will be introduced and used as basic in this paper to tackle the constraints of IMs using MPC in real time.

C. Constraint Reformulation

In FOC, the stator-voltage equations for the inner loop are given by

$$u_{sd} = R_s i_{sd} + \sigma L_s \dot{i}_{sd} + (1-\sigma) L_s \dot{i}_{\mu} - \omega_e \sigma L_s i_{sq}$$
$$u_{sq} = R_s i_{sq} + \sigma L_s \dot{i}_{sq} + (1-\sigma) L_s \omega_e i_{\mu} + \omega_e \sigma L_s i_{sd} \tag{10}$$

with the constraints

$$i_{sd}^2 + i_{sq}^2 \le I_{dq\_\max}^2 \quad \text{and}$$
$$u_{sd}^2 + u_{sq}^2 \le U_{dq\_\max}^2 \tag{11}$$

where R_s, L_s σ, and ω_e denote the stator resistance, stator inductance, flux-leakage coefficient, and the synchronous speed. i_{sd}, i_{sq}, u_{sd}, u_{sq} represent the stator currents and voltages in *dq*-frame. $I_{dq\_\max}$ and $U_{dq\_\max}$ are the maximum admissible stator current and available inverter voltage converted into *dq*-frame, respectively.

It is obviously that (11) does not fulfill the linear inequality specified in (9). In order to describe the problem in QP form, the constraints are approximated by polygons, whereby the quadratic inequality is replaced by a set of linear ones. The higher the degree of the polygon is specified, the more accurate is the approximation. On the other hand, more inequalities are generated, which raises the computational effort. In order to overcome this drawback, the system constraints of IMs will be reformulated.

To convert the quadratic inequality system constraints to linear one, the torque limit of the system is regarded. The available maximum torque can be determined by the following equations:

$$I_{dq\_\max}^2 = i_{sd}^2 + i_{sq}^2 \tag{12}$$
$$U_{dq\_\max}^2 = (\omega_e L_s i_{sd})^2 + (\omega_e L_{\sigma s} i_{sq})^2 \tag{13}$$
$$i_{sd} = \frac{\omega_N}{\omega_R} i_{sd\_N} \tag{14}$$
$$T_e = \frac{pL_m^2}{L_r} i_{sd} i_{sq} \tag{15}$$

where

- ω_N nominal electrical rotor speed;
- ω_R actual electrical rotor speed;
- $L_{\sigma s}$ stator-leakage inductance;
- L_m mutual inductance;
- L_r rotor inductance referred to the stator side;
- i_{sd_N} nominal stator *d*-current referred to synchronous frame;
- T_e air-gap torque;
- p pole-pair number of IM.

Because the voltage limit is taken into account only in the field-weakening area, where the voltage drops on stator and rotor resistances are much smaller when compared to the induced voltage due to rotation, the voltage boundary line described in (10) and (11) can be simplified in the form of (13). The direct current element i_{sd} is used instead of the magnetizing current i_μ, since the excess of current limitation in transient states should be considered as well and the applied voltage can be limited by available dc-link voltage of the inverter. In this paper, the conventional constant-rotor-flux method with field-weakening in (14) is applied for the torque-limit calculation.

In consideration of (12), (14), and (15) in basic speed area and (13)–(15) in the field-weakening area, the system constraint on the torque can be described by

$$-\overline{T_e} \le T_e \le \overline{T_e}, \text{ where } \overline{T_e}$$
$$= \begin{cases} \frac{pL_m^2}{L_r} i_{sd\_N} \sqrt{I_{dq\_\max}^2 - i_{sd\_N}^2} & \text{(16a)} \\ \frac{pL_m^2}{L_r} \frac{\omega_N}{\omega_R} i_{sd\_N} \sqrt{\left(\frac{U_{dq\_\max}}{\omega_e L_{\sigma s}}\right)^2 - \left(\frac{\omega_N}{\sigma \omega_R} i_{sd\_N}\right)^2} & \text{(16b)} \end{cases}$$

where (16a) describes the maximum torque of the IM, which has a constant value and is only available in basic speed area. In the field-weakening area, the maximum torque depends on the actual rotor speed ω_R and ω_e, which represents the synchronous frame speed at the operating point of actual rotor speed and maximum torque application, specified in (16b). However, ω_e is not directly given in the control strategy, which is dependent on the equation

$$\omega_e = \frac{R_r i_{sq}}{L_r i_{sd}} + \omega_R \tag{17}$$

where R_r and L_r are the rotor resistance and inductance, respectively. ω_e can then be expressed by ω_R by an analytical solution of (13)–(17). The torque constraint formulation in field-weakening area is thereby only with respect to ω_R by substituting this solution in (16b). For a given rotor speed ω_R, the torque limit can be then determined by solving a fourth-order polynomial equation.

Furthermore, it has to be considered that the voltage limit (13) is represented by i_{sd}. In case of field-weakening operation, the magnetizing current i_μ drops slower than i_{sd} in transient states, so that the actual electromotive force (EMF) in the *q*-axis

$$\epsilon_q = \omega_e \sigma L_s i_{sd} + (1-\sigma)\omega_e L_s i_\mu \tag{18}$$

resulted primarily by i_{sd} and i_μ is larger than the one calculated merely by i_{sd}. As a consequence, the voltage in the IM is larger than the voltage limit in transient states in the field-weakening area. This issue can be suppressed by applying i_μ in the voltage-limit calculation and using a rotor-flux controller, whereat current overshoot can arise in transient procedures and the current limit would be exceeded. In contrast, the impact of resulted applied overvoltage in transient states in this case can be limited by available dc-link voltage of the inverter as mentioned before. Therefore, the flux controller is abandoned in this paper.

III. Explicit Model Predictive Speed Control of IMs

By online optimization of problem (9), the value of $\hat{x}_t$ is given at each time step for the solution. Therefore, the control law $u = u(t)$ is defined implicitly as a function of $\hat{x}_t$. To reduce the computational effort, the EMPC is introduced in this paper. The EMPC based on mp-QP, which was proposed in [37], solves the QP for all $x(t)$ offline to find the control law $u = u(x)$ explicitly. According to the actual value of $x(t)$, the solution is calculated online by means of the explicit form. By extension of standard mp-QP form for reference tracking, we convert the constraint formulated in (16), which does not match the linear inequality, into a linear one.

A. Multiparametric QP

The standard QP can be converted into mp-QP in such a way that state variables are treated as a vector of parameters. According to the constraints, the space of the parameters can be defined by a set of regions, which are convex polyhedral and in which the QP is feasible. The control law by solving the optimization problem is then expressed piecewise with respect to the vector of the parameters. It is proved that the linear MPC controller is a continuous PWA function of the parameters [37].

To introduce the algorithm of mp-QP, we consider at first the QP of regulation problem with measurable state variables and having cost function

$$\widetilde{J} = \boldsymbol{x}_{t+N_p}^T P \boldsymbol{x}_{t+N_p} + \sum_{k=0}^{N_p-1} \left(\boldsymbol{x}_{t+k}^T Q \boldsymbol{x}_{t+k} + \boldsymbol{u}_{t+k}^T R \boldsymbol{u}_{t+k} \right). \tag{19}$$

As the derivation in Section II, we obtain the following QP from (19)

$$\begin{aligned} V(\boldsymbol{x}) = \min_{\boldsymbol{U}} & \left\{ \frac{1}{2} \boldsymbol{U}^T H \boldsymbol{U} + \boldsymbol{x}_t^T F \boldsymbol{U} \right\} \\ \text{s.t. } & G\boldsymbol{U} \leq b + E\boldsymbol{x}_t \,. \end{aligned} \tag{20}$$

By defining $\boldsymbol{z} \triangleq \boldsymbol{U} + H^{-1} F^T \boldsymbol{x}_t$ and substituting it in (20), we attain an equivalent problem

$$\begin{aligned} V_{\boldsymbol{z}}(\boldsymbol{x}) = \min_{\boldsymbol{z}} & \frac{1}{2} \boldsymbol{z}^T H \boldsymbol{z} \\ \text{s.t. } & G\boldsymbol{z} \leq b + S\boldsymbol{x}_t \end{aligned} \tag{21}$$

where $S \triangleq E + GH^{-1}F^T$ and $V_{\boldsymbol{z}}(\boldsymbol{x}) = V(\boldsymbol{x}) + \frac{1}{2}\boldsymbol{x}_t^T F H^{-1} F^T \boldsymbol{x}_t$. Compared to (20), the parameter vector $\boldsymbol{x}_t$ in (21) stands only on the right side of the inequality. In [37], it is proved that $\boldsymbol{z}$ is also an affine function of parameter vector $\boldsymbol{x}$. Fulfilling both primal and dual feasibility, the constraints can be converted to linear inequalities of the parameter vector. According to these inequalities, the parameter vector space can be partitioned into a set of convex polyhedral regions called critical regions, in which the problem is feasible. They are described by

$$CR_i = \{ \boldsymbol{x} \in \Re^n | H_i \boldsymbol{x} \leq K_i \} \,. \tag{22}$$

The optimum solution can be obtained as a PWA function in following form:

$$\boldsymbol{u}^* = f_i \boldsymbol{x} + g_i \,. \tag{23}$$

Now we return to our problem. By combining (9) and (16), the problem can be summarized as follows:

$$\begin{aligned} \min_{\boldsymbol{U}} & \left\{ \frac{1}{2} \boldsymbol{U}^T H \boldsymbol{U} + [\hat{\boldsymbol{x}}_t^T \; \boldsymbol{w}_t^T] F \boldsymbol{U} \right\} \\ \text{s.t. } & \begin{bmatrix} I \\ -I \end{bmatrix} \boldsymbol{U} \leq E \begin{bmatrix} \overline{T_e} \\ \overline{T_e} \end{bmatrix} \end{aligned} \tag{24}$$

where $[\hat{\boldsymbol{x}}_t^T \; \boldsymbol{w}_t^T] F = c^T$. In order to obtain the formulation described in (20), we redefine our parameter vector as

$$\tilde{\boldsymbol{x}}_t = \begin{bmatrix} \hat{x}_t \\ w_t \\ \overline{T_e} \\ \overline{T_e} \end{bmatrix} . \tag{25}$$

Then, (24) is transformed into

$$\begin{aligned} \min_{\boldsymbol{U}} & \left\{ \frac{1}{2} \boldsymbol{U}^T H \boldsymbol{U} + \tilde{\boldsymbol{x}}_t^T \tilde{F} \boldsymbol{U} \right\} \\ \text{s.t. } & \begin{bmatrix} 0 \\ 0 \\ I \\ -I \end{bmatrix} \boldsymbol{U} \leq \tilde{E} \tilde{\boldsymbol{x}}_t \end{aligned} \tag{26}$$

which fulfills the form of (20).

B. Controller Design

The model predictive speed controller for IMs is designed by taking into account the load disturbance as additional state variable in order to get offset-free reference speed tracking. A Kalman filter is applied to correct the predicted state variables in consideration of state and output disturbances at each time step. It is designed by using the form

$$\begin{cases} \begin{bmatrix} x_{t+1} \\ d_{t+1} \end{bmatrix} &= \begin{bmatrix} A & B_d \\ 0 & I \end{bmatrix} \begin{bmatrix} x_t \\ d_t \end{bmatrix} + \begin{bmatrix} B \\ 0 \end{bmatrix} u_t \\ y_t &= \begin{bmatrix} C & C_d \end{bmatrix} \begin{bmatrix} x_t \\ d_t \end{bmatrix} \end{cases} \tag{27}$$

where B_d and C_d represent the matrices of state and output disturbances, respectively. The state variable x and system matrices A, B, and C are the same as MPC's and are defined as follows: $x = \omega_R$, $A = 1$, $B = \frac{p \cdot T_s}{J}$, and $C = 1$. It should be considered that the disturbance estimated from the observer has to be compensated to the electrical rotor speed, because the torque u_t computed by the EMPC controller is hard limited by system constraints. The sampling time T_s in this system is defined by 0.1 ms.

Since the system constraints have been already considered in the speed control design, an unconstrained MPC is constructed as current controller using the following formulation:

$$\begin{bmatrix} i_{sd} \\ i_{sq} \end{bmatrix}_{t+1} = \begin{bmatrix} 1 - \frac{Rs \cdot T_s}{\sigma L_s} & 0 \\ 0 & 1 - \frac{Rs \cdot T_s}{\sigma L_s} \end{bmatrix} \begin{bmatrix} i_{sd} \\ i_{sq} \end{bmatrix}_t + \begin{bmatrix} \frac{T_s}{\sigma L_s} \\ \frac{T_s}{\sigma L_s} \end{bmatrix} \boldsymbol{u}_t . \tag{28}$$

The EMF compensation is added additionally to the system input. As for the speed loop, a Kalman filter with disturbance modeling like in (27) is applied to get an offset-free tracking and enhance the robustness against uncertainties. However, the estimated disturbance has to be compensated in this case to the system input, since the currents are hard constrained.

Fig. 3 shows the block diagram of the whole control structure. The explicit expression of control laws is computed offline. According to the actual rotor speed, the torque limit value is calculated online based on the formulations introduced in Section II-C. The Kalman filter is integrated into the EMPC

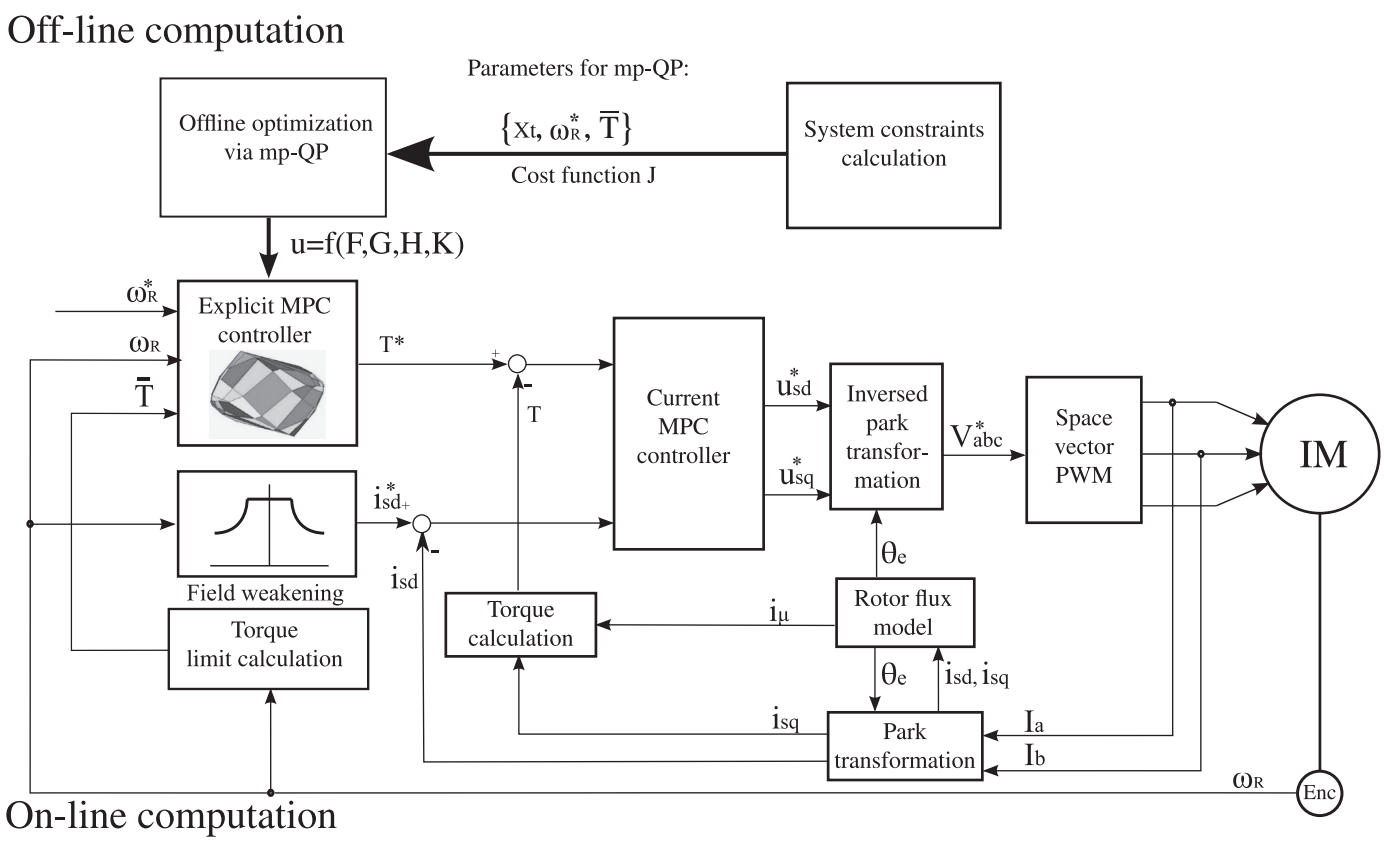

Fig. 3. Block diagram of the control structure with EMPC.

controller and therefore not presented in this block diagram. By using the actual values of the parameter vector introduced in (25), the actual critical region is searched and the corresponding control law is calculated online. There is no system-constraint consideration and approximation needed anymore in the current controller. Furthermore, the flux controller is abandoned in the control design in order to prevent from current overshooting in transient procedures. Certainly, the system dynamic is reduced a bit as the sacrifice.

The parameters of our MPC problem (9) transformed into (26) are defined by

$$N_p = 7, \quad N_u = 1, \quad Q = 1, \quad R = 1 \times 10^{-3} \tag{29}$$

with covariance matrices of state and output variables

$$Q_a = \text{diag}(\text{ones}(1,2)), \quad R_a = 1 \times 10^4 \tag{30}$$

for the simulation, and

$$N_p = 7, \quad N_u = 1, \quad Q = 1, \quad R = 0.4 \tag{31}$$

with covariance matrices

$$Q_a = \text{diag}(\text{ones}(1,2)), \quad R_a = 5 \times 10^5 \tag{32}$$

for the test bench.

To solve the mp-QP depicted in (26) with dynamic constraint, the MATLAB Toolbox YALMIP [41] is utilized in this study, in which the multiparametric toolbox (MPT) [42] is invoked. The solution of the proposed problem consists of control laws defined in 20 polyhedral regions in $\Re^3$ state space. Fig. 4(a) and (b) illustrates the critical regions projected, respectively, on the plane surfaces $[x \ w]$ with $\overline{T_e} = 50$ Nm and $[x \ \overline{T_e}]$ with $w = 150$ rad/s. The explicit control laws of the MPC controller are shown in Fig. 5, which can be identified as a PWA function of the parameter vector in each region, respectively.

IV. Simulation Results

The parameters given in Table I are used both for the simulation and on the test bench. The sampling time of the simulation is configured by $T_s = 0.1$ ms. In order to reduce the online computational effort, the analytical calculation of torque limit introduced in Section II-C and shown in Fig. 3 would be moved offline.

Fig. 6 illustrates the offline computation results of torque limit, which is stored in a look-up table and applied for the online computation. The purpose of this paper is to show and validate the new method of constraint handling of IMs using MPC. Since the same drive cycle will be utilized for both the simulation and the test bench, the system constraints are newly defined in order to prevent from electrical and mechanical damage, which is shown in Table I. Therefore, the system dynamic will be diminished. However, it should be focused on in this paper that the system resource is optimally organized under the new constraint condition.

The simulation runs as follows. Initially, the reference rotor speed is changed abruptly to 1400 r/min, whereat the load ramps up from 0 to 55 Nm within the first 9 s. After 10 s, the

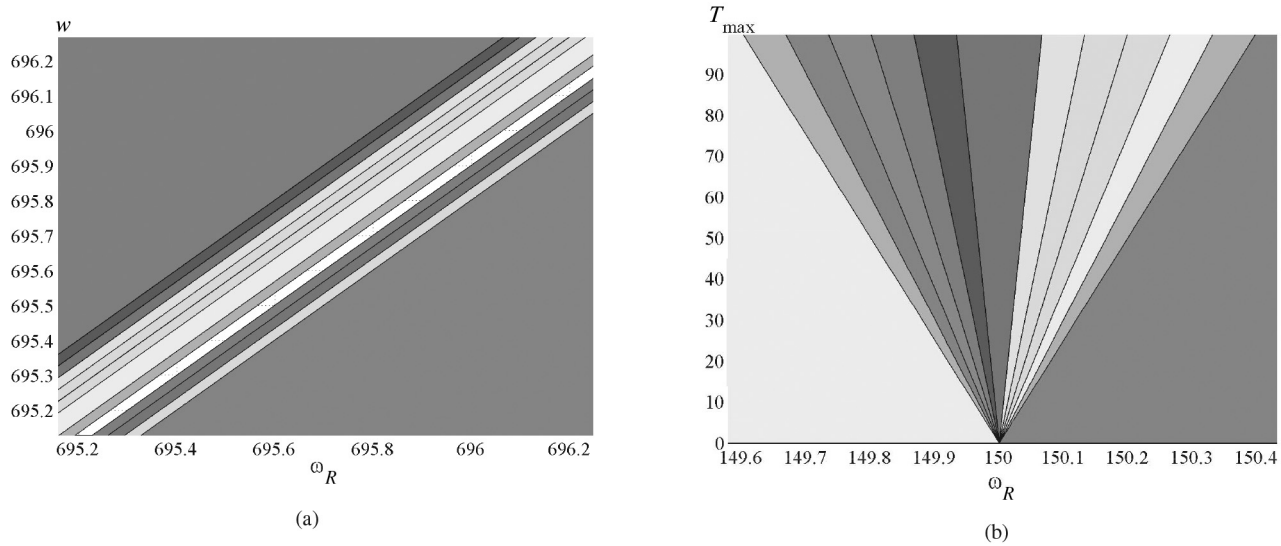

Fig. 4. State-space partition. (a) State-space partition over $[\omega_R \;\; w]$-subspace. (b) State-space partition over $[\omega_R \;\; \overline{T_e}]$-subspace.

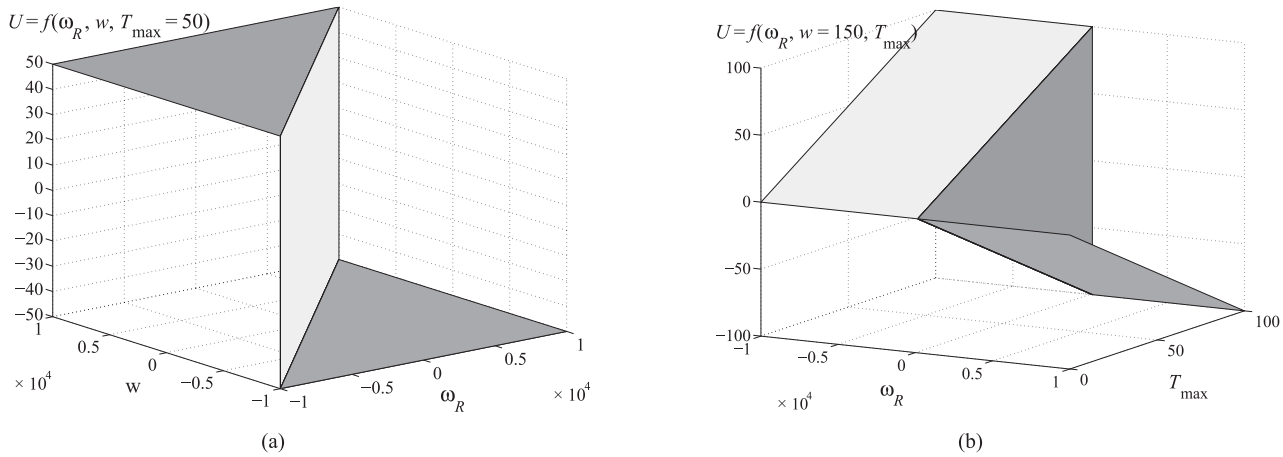

Fig. 5. Explicit control law. (a) Explicit control law $u^*(x)$ in $[\omega_R \;\; w]$-subspace. (b) Explicit control law $u^*(x)$ in $[\omega_R \;\; \overline{T_e}]$-subspace.

TABLE I
IM PARAMETERS FOR THE STUDY

$U_{\mathrm{dq\_max}}$	$200\sqrt{2}$ V	$I_{\mathrm{dq\_max}}$	40 A
$i_{\mathrm{sd\_}N}$	21.26 A	T_N	56 Nm
ω_N	309.4 rad/s	Pole number	4
R_s	0.29 Ω	R_r	0.1232 Ω
L_s	42 mH	L_r	41.4 mH
L_m	40.1 mH	σ	0.0754

load torque falls to 12 Nm. A few seconds later, the reference speed is increased to 2000 r/min in step form, which is larger than the rated speed.

As shown in Fig. 7, the MPC controller demands the maximum torque, which is limited to 56 Nm in the basic speed area, as long as the reference speed is not reached. Once the rotor speed is equal to the reference value, the required drive torque drops to the actual value of the load torque and follows it. In the phase of speed increase from 1400 to 2000 r/min, which is mainly in the field-weakening area, the reference torque

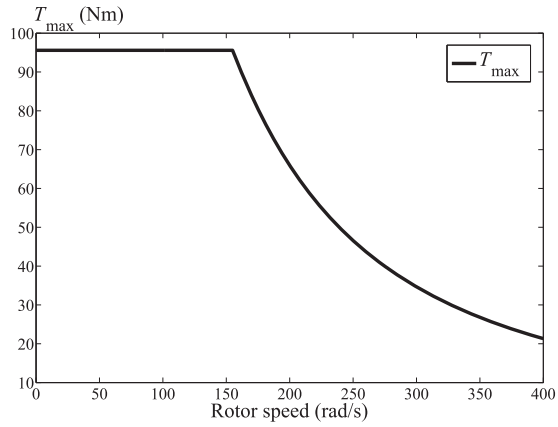

Fig. 6. Result of torque-limit calculation.

required by the MPC controller coincides with the curve shown in Fig. 6 in the field-weakening area. As soon as the transient procedure is finished, the reference torque is reduced to the load torque again.

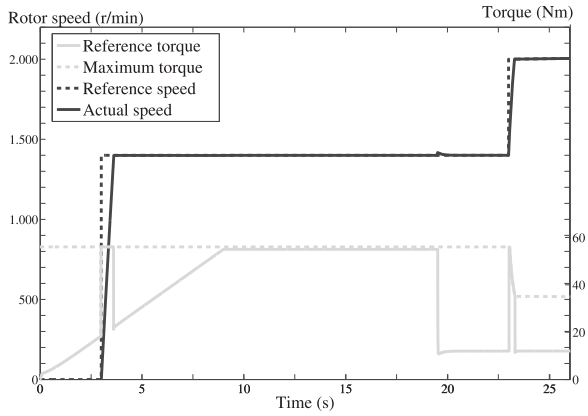

Fig. 7. Rotor speed–reference torque.

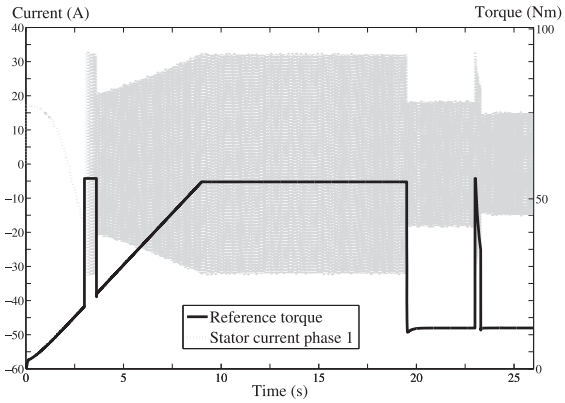

Fig. 8. Stator current–reference torque.

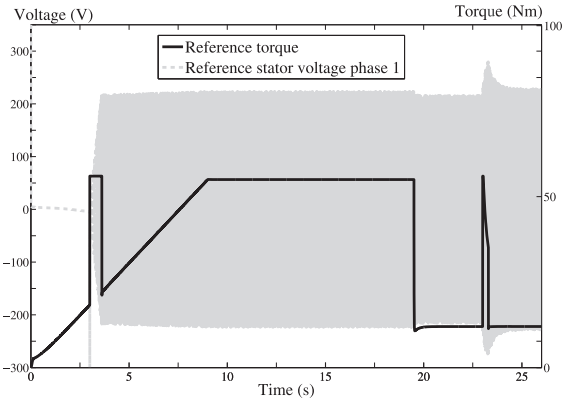

Fig. 9. Stator voltage–reference torque.

Fig. 8 shows the stator current change in the simulation. According to Table I, the admissible amplitude of the phase current $\widehat{I}_{abc}$ corresponding to $I_{dq\_\max}$ is calculated to be 32.7 A. The maximum current by dint of $1/\omega_R$ method is delivered when the maximum torque is required in the basic speed area. As shown in Fig. 8, the amplitude of the current is well limited to $\widehat{I}_{abc}$ by using the torque constraint.

The admissible amplitude of the phase voltage $\widehat{U}_{abc}$ is calculated analogically as by $\widehat{I}_{abc}$, whose value is equal to 231 V. As mentioned in Section II-C, the voltage limit is first considered in the field-weakening area. The maximum voltage is demanded in the case of maximum torque requirement in the field-weakening area. In Fig. 9, it is presented that the maximum voltage is reached at the nominal point. However, during the transient procedure of the field-weakening operation in case of maximum torque requirement, the stator voltage exceeds the limit value. The clarification of this phenomenon has been given in Section III, which is confirmed in Fig. 10.

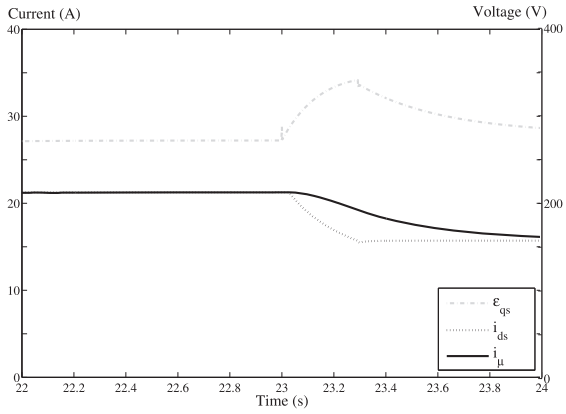

Fig. 10. Overshooting of ϵ_q due to i_{sd} and i_μ.

In the following, the comparisons between proposed approach and PI controller as well as EMPC with approximated constraints are given. To compare the dynamics of the proposed EMPC controller and the PI controller, the following reference speeds are applied in sequence: 500, 600, 650, 675, and 680 r/min. The offsets from each reference-value change are reduced step by step. The parameters of the PI current and speed controllers are tuned by means of magnitude and symmetric optimum, respectively. The IM is driven without load. Fig. 11(a)–(e) shows the step responses with different step changes, respectively. The PI controller achieves comparable dynamic as the proposed EMPC in the case of large reference change. Because of the significant control deviation, the maximum permissible torque is applied by the PI controller as shown in Fig. 11(a). However, the manipulated value of the PI controller reduces when the reference change gets smaller. The smaller the step change is, the smaller is the reference torque applied by the PI controller, which is illustrated in Fig. 11(b)–(e). Generally, the parameter optimization of the PI controller can only be designed within a constricted operating range. In contrast, the proposed approach applies the maximum permissible torque independent on the size of reference change to obtain the high dynamic.

To present the advantage of the proposed EMPC approach compared to the EMPC with approximated constraints, the following constraints are defined:

$$\begin{aligned} 0 \le\ & i_{sd} \le\ & i_{sd\_N} \\ -\sqrt{I_{dq\_\max}^2 - i_{sd\_N}^2} \le\ & i_{sq} \le\ & \sqrt{I_{dq\_\max}^2 - i_{sd\_N}^2} \\ -\frac{U_{dq\_\max}}{\sqrt{2}} \le\ & u_{sd} \le\ & \frac{U_{dq\_\max}}{\sqrt{2}} \\ -\sqrt{U_{dq\_\max}^2 - u_{sd\_\mathrm{ref}}^2} \le\ & u_{sq} \le\ & \sqrt{U_{dq\_\max}^2 - u_{sd\_\mathrm{ref}}^2}. \end{aligned} \tag{33}$$

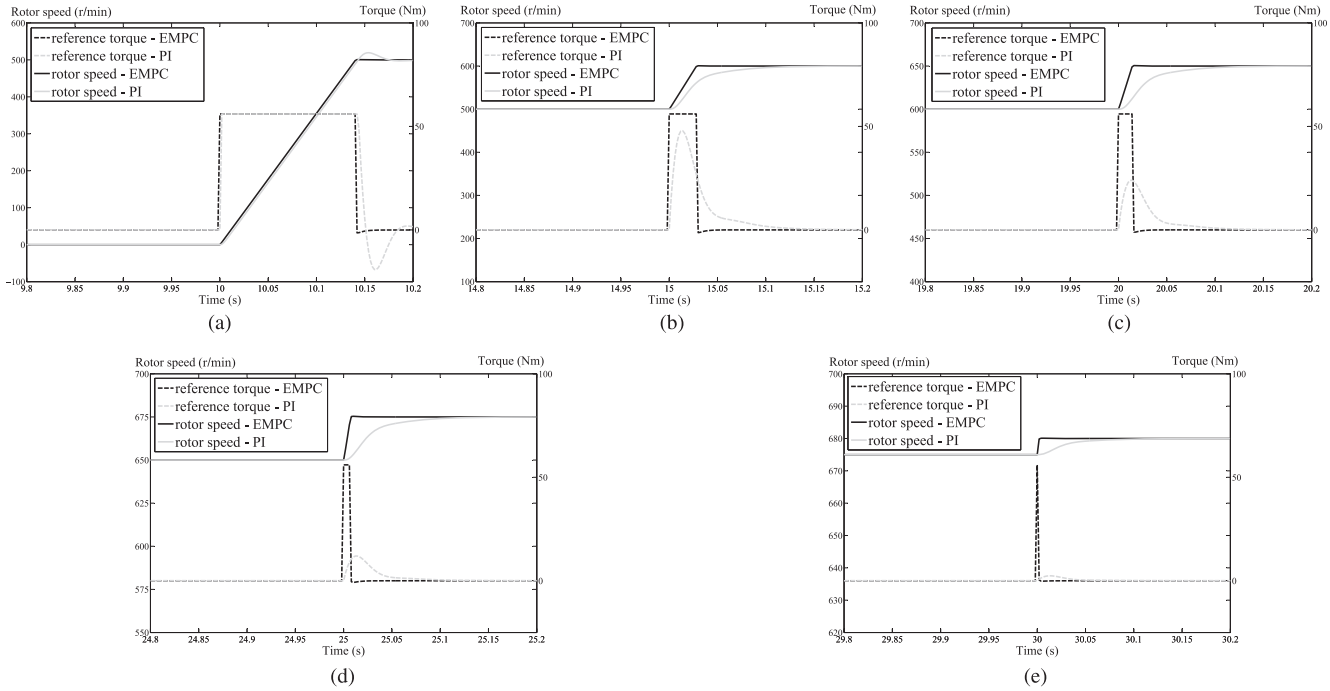

Fig. 11. Optimality comparison between EMPC and PI. (a) Step change $= 500$ r/min. (b) Step change $= 100$ r/min. (c) Step change $= 50$ r/min. (d) Step change $= 25$ r/min. (e) Step change $= 5$ r/min.

The stator current on the d-axis i_{sd} is limited by the nominal magnetizing current and should be larger and equal to zero, where the q-component of the stator current i_{sq} is constrained by the positive and negative value of the rated current on the q-axis. Since the stator voltage on the d-axis is much smaller than the one on the q-axis at high speed due to the leakage factor, it is constrained by a constant value, whereas the constraint of the q-component voltage is determined by the maximum voltage and the actual reference voltage on the d-axis. Therefore, both the current and voltage constraints are approximated by polygons in the form of rectangles. Because the dq-components of stator current and voltage are decoupled, two EMPC controllers are able to be implemented separately to reduce the dimension of the state space. The torque constraint of the speed controller is given by the rated torque. After the offline optimization, 29 polyhedral regions in $\Re^3$ state space are defined for each EMPC current controller.

The simulation result of the proposed EMPC approach and the EMPC with the approximated constraints defined in (33) is presented in Fig. 12. At first, the reference speed is set by 1400 r/min, which is in the basic speed area. In this area, the system is only constrained by the current inequalities, because the stator current on the d-axis remains at its rated value, which means that the maximum torque is reachable for both approaches. Therefore, there is no difference of system dynamics between both approaches as shown in the figure. Then, the reference speed rises to 2000 r/min, which lies in the field-weakening area and the voltage constraints should be taken into account. In the optimization of EMPC with approximated constraints, only the area inside the rectangle defined by the voltage inequalities is feasible, whereas the feasible area of the proposed approach is represented by the voltage ellipse

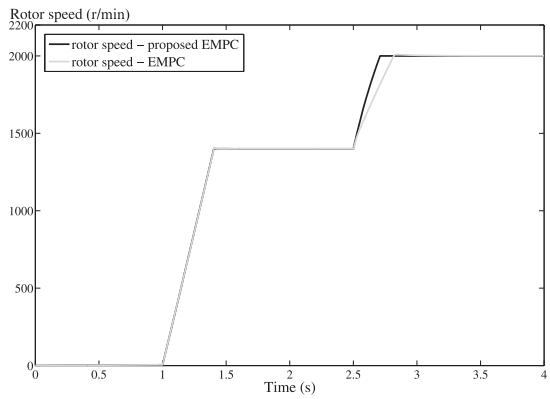

Fig. 12. Dynamics comparison between proposed EMPC and EMPC with approximated constraints.

defined by the original voltage description derived from (10) and (11). Therefore, less system resource, i.e., voltage in case of field-weakening, can be used by the EMPC with approximated constraints. Due to this issue, the system dynamic is impacted by the approximation as shown in the figure. As mentioned before, the performance can be improved if the approximation is more accurate. However, the hexagonal approximations of current and voltage constraints lead to 1057 polyhedral regions, since the dq-components are no more decouplable due to the inequality formulations. Thereby, the online computational effort is enhance significantly, whereat the feasible area is still smaller than the proposed approach.

V. Experimental Results

The simulation results presented in Section IV exhibit a good performance concerning constraint handling. In this section,

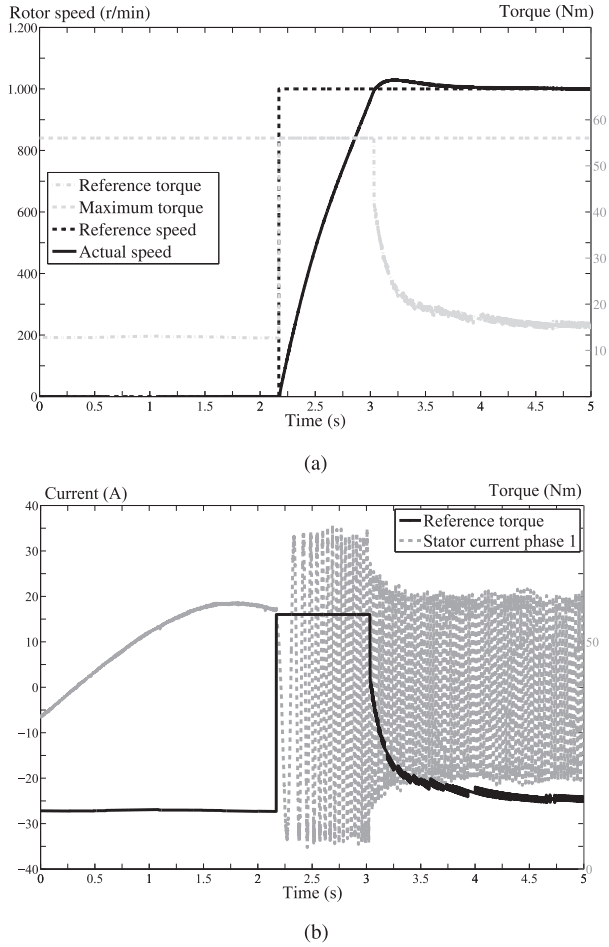

Fig. 13. Start up. (a) Rotor speed–reference torque. (b) Stator current–reference torque.

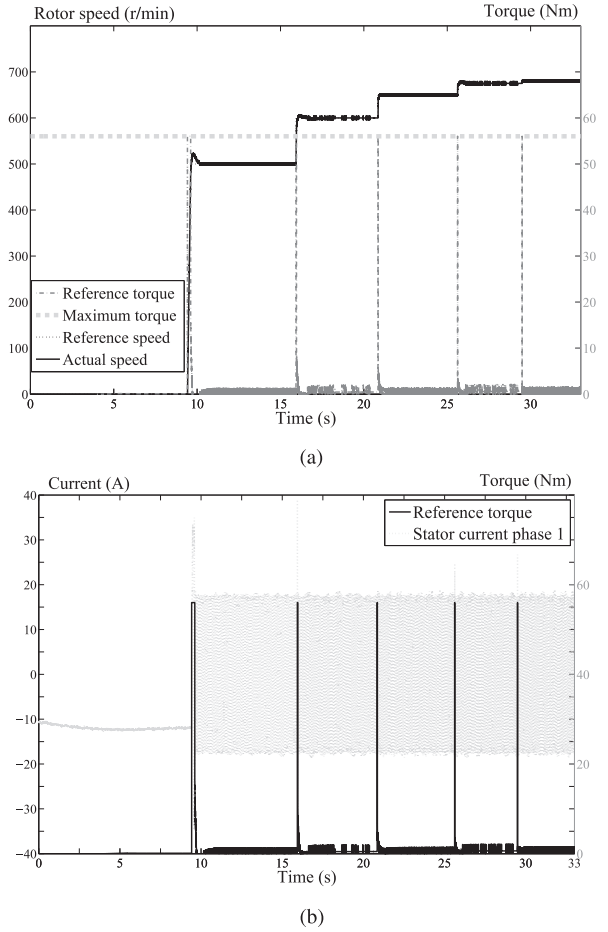

Fig. 14. Diverse speed requirements. (a) Rotor speed–reference torque. (b) Stator current–reference torque.

the proposed method will be validated on a laboratory test bench, which is composed of an IM with four poles with nominal power of 22 kW driven by a voltage-source inverter and a permanent-magnet synchronous machine (PMSM) with six poles. The parameters on the data sheets of both machines can be found in the appendix. The control algorithm is implemented on a digital signal-processor (DSP) platform using dSPACE 1103 hardware. The sampling time of the system is defined as same as in the simulation. As mentioned before, the voltage and current limits for the validation are redefined for safety reasons as in Table I.

In the following, the results of three tests will be presented: the first test shows the current limit by dint of the proposed method in a start-up process; the second test indicates the optimality of the implementation; the last test delivers the measurement results to be compared to the simulation results.

In the start-up test, a load torque of 13 Nm is imposed to the shaft. Then, the reference speed is changed to 1000 r/min. As shown in Fig. 13(a), the reference torque calculated by the speed controller jumps to the maximum available torque at the same time. The reference torque falls to the value equal to the load torque after the transient procedure is terminated. Parallelly, as shown in Fig. 13(b), the stator current is well limited in the whole process, especially in the transient procedure. The amplitude of the stator current shown in the figure is below 35 A, which is a bit higher than the theoretical limit due to the noises.

In the second test, the IM is driven as in the simulation with different step changes, in order to check the optimality of the control algorithm. In Fig. 14(a), it is evident that despite of the diminished offsets, the maximum admissible torque is enforced for each transient procedure. It confirms that the maximum system resource is required no matter how large the offset is, which implicates the optimality of the control algorithm. The stator current curve is illustrated in Fig. 14(b). The current is limited to the admissible current except in the second transient procedure. However, the current limit is exceeded for about 5 ms and the peak value is about 39 A. Usually, the admissible peak current of power electronics is much higher than the one for continuous operations. Therefore, the exceeding in this case will not plague the hardware and is not critical. In case of maximum torque requirement for long durations, no overcurrent will arise, which is depicted in the first test.

In the last test, the similar drive cycle is executed. The load torque ramps from the beginning until 55 Nm. Due to the signal noises, the maximum admissible torque is not applied to the load. The reference speed is set to 1400 r/min same as in the simulation. After the steady state is reached, the load is changed

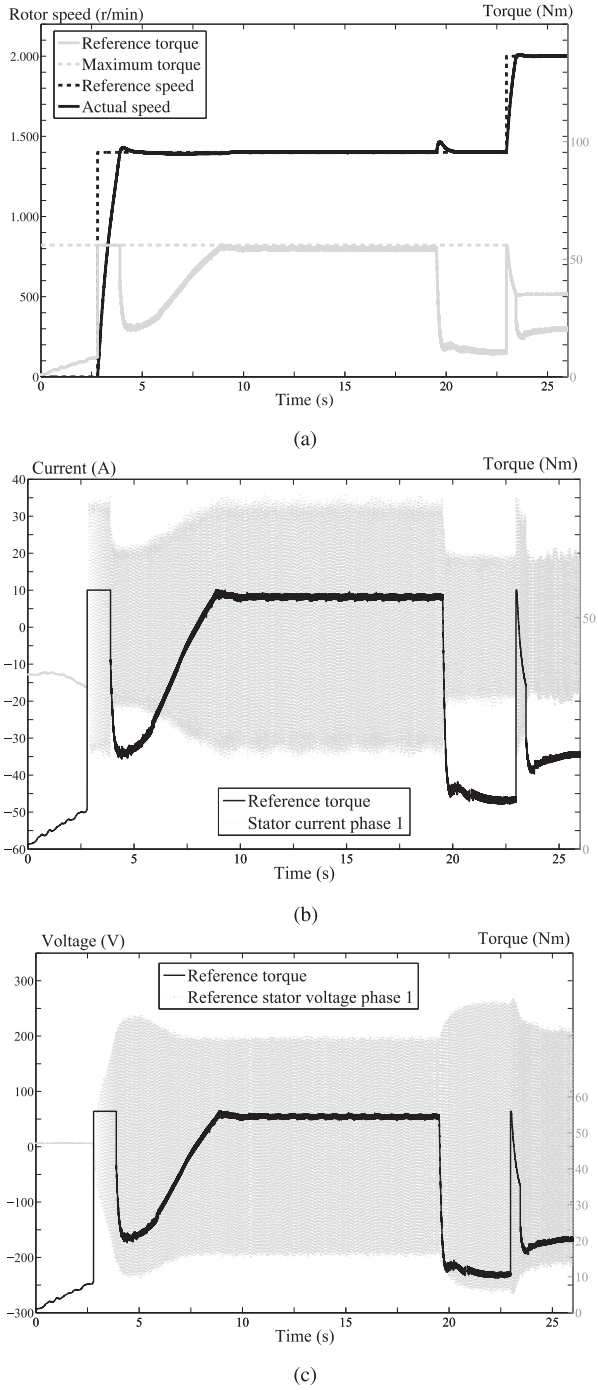

Fig. 15. Drive cycle. (a) Rotor speed–reference torque. (b) Stator current–reference torque. (c) Stator voltage–reference torque.

from 55 to 12 Nm. After a few seconds, the reference speed is set to be 2000 r/min as in the simulation.

In Fig. 15, the experimental results are shown. In the first phase, about in the first 2.8 s in Fig. 15(a), the reference torque follows the load because no control offset exists. As soon as the reference speed changes to 1400 r/min, the speed controller enforces the reference torque to the maximum torque in order to reach the reference value as quickly as possible. Once the reference value is met, the reference torque drops to the current load torque and increases with it. At about the 20th second, the load drops to 12 Nm. After the reference speed is required to 2000 r/min, the reference torque rises first to 56 Nm and then follows the maximum torque curve since entering the field-weakening area until the reference speed is reached. This measurement result coincides with the simulation result presented in Section IV.

The stator current curve in one phase is presented in Fig. 15(b). As the maximum admissible torque is required at the third second, the stator current reaches its limit. From the 9th second to the 19th second, the stator current remains around the current limit, as the load is approximately equal to the maximum torque. In the next procedure of maximum torque requirement, the stator current rises to the limit and then drops because of the field-weakening operation. Thus, the current limit via torque limit is validated.

The reference values of the stator voltage are described in Fig. 15(c). Since the IM is in standstill at the beginning, the stator voltage results mainly from the voltage drop of the stator resistor on the d-axis, which is marginal compared to its limiting value. Due to the little speed overshooting shown in Fig. 15(a), the voltage limit is arrived at around the 5th second. Because of the load reduction at the 20th second, the rated speed is exceeded, so that the maximum voltage is reached again. Due to the maximum torque requirement in the field-weakening area around the 23rd second, the reference voltage exceeds the maximum admissible voltage, which confirms the explanation in Section II and agrees with the simulation result. Consequently, the control algorithm with the proposed constraint handling is validated by the experimental results.

VI. Conclusion

In this paper, it was attained that the system constraints can be considered without approximation by polygons when using MPC controllers for IMs, and the controller has to work in real time. By means of the reformulation of the system constraints with respect to the maximum admissible torque and mp-QP for reference tracking with extension of an additional variable, an EMPC controller was designed, which fulfills these requirements. This method is suitable not only for speed-controlled IMs but also for torque-controlled IMs, in which the output constraints should be handled instead (see [4]). The variation in the system parameters is not considered in this work and is handled separately in [43].

References

[1] P. Vas, *Vector Control of AC Machines*. Oxford, U.K.: Clarendon, 1990.
[2] O. Föllinger, *Regelungstechnik*, 10th ed. Heidelberg, Germany: Hüthig GmbH Verlag, 2008.
[3] A. Linder, R. Kanchan, and R. Kennel, and P. Stolze, *Model-Based Predictive Control of Electric Drive*. Göttingen, Germany: Cuvillier Verlag, 2010.
[4] E. F. Camacho and C. Bordons, *Model Predictive Control*. New York, NY, USA: Springer, 2013.
[5] M. Morari and J. H. Lee, "Model predictive control: Past, present and future," *Comput. Chem. Eng.*, vol. 23, nos. 4–5, pp. 667–682, May 1999.
[6] J. H. Lee, "Model predictive control: Review of the three decades of development," *Int. J. Control Autom. Syst.*, vol. 9, no. 3, pp. 415–424, 2011.

[7] J. Richalet, A. Rault, J. L. Testud, and J. Papon, "Model predictive heuristic control: Applications to industrial processes," *Automatica*, vol. 14, no. 5, pp. 413–428, Sep. 1978.
[8] C. R. Cutler and B. C. Ramaker, "Dynamic matrix control—A computer control algorithm," in *Proc. Autom. Control Conf.*, San Francisco, CA, USA, 1980, pp. WP5-B.
[9] C. E. García, D. M. Prett, and M. Morari, "Model predictive control: Theory and practice—A survey," *Automatica*, vol. 25, no. 3, pp. 335–348, May 1989.
[10] S. S. Keerthi and E. G. Gilbert, "Optimal infinite horizon feedback laws for a general class of constrained discrete-time systems: Stability and moving horizon approximations," *J. Optim. Theor. Appl.*, vol. 57, no. 2, pp. 265–293, May 1988.
[11] J. B. Rawlings and K. R. Muske, "The stability of constrained receding horizon control," *IEEE Trans. Automat. Control*, vol. 38, no. 10, pp. 1512–1516, Oct. 1993.
[12] H. Chen and F. Allgöwer, "A quasi-infinite horizon nonlinear model predictive control scheme with guaranteed stability," *Automatica*, vol. 34, no. 10, pp. 1205–1217, Oct. 1998.
[13] J.-W. Lee, "Exponential stability of constrained receding horizon control with terminal ellipsoid constraints," *IEEE Trans. Automat. Control*, vol. 45, no. 1, pp. 83–88, Jan. 2000.
[14] D. Q. Mayne, J. B. Rawlings, C. V. Rao, and P. O. M. Scokaert, "Constrained model predictive control: Stability and optimality," *Automatica*, vol. 36, no. 6, pp. 789–814, Jun. 2000.
[15] A. Saberi and A. Stoorvogel, and P. Sannuti, *Control of Linear Systems With Regulation and Input Constraints*. New York, NY, USA: Springer, 2000.
[16] T. Besselmann, J. Löfberg, and M. Morari, "Explicit MPC for LPV systems: Stability and optimality," *IEEE Trans. Automat. Control*, vol. 57, no. 9, pp. 2322–2332, Sep. 2012.
[17] N. Kutasi, A. Kelemen, and M. Imecs, "Vector control of induction motor drives with model based predictive current controller," in *Proc. Int. Conf. Comput. Cybern. (ICCC)*, Stara Lesna, Slovakia, 2008, pp. 21–26.
[18] L. Gan and L. Wang, "Cascaded model predictive position control of induction motor with constraints," in *Proc. 39th Annu. Conf. IEEE Ind. Electron. Soc. (IECON)*, Vienna, Austria, 2013, pp. 2656–2661.
[19] P. Alkorta, O. Barambones, J. A. Cortajarena, and A. Zubizarrreta, "Efficient multivariable generalized predictive control for sensorless induction motor drives," *IEEE Trans. Ind. Electron.*, vol. 61, no. 9, pp. 5126–5134, Sep. 2014.
[20] C. S. Lim, E. Levi, M. Jones, N. A. Rahim, and W. P. Hew, "FCS-MPC-based current control of a five-phase induction motor and its comparison with PI-PWM control," *IEEE Trans. Ind. Electron.*, vol. 61, no. 1, pp. 149–163, Jan. 2014.
[21] H. Guzman, M. J. Duran, F. Barrero, B. Bogado, and S. Toral, "Speed control of five-phase induction motors with integrated open-phase fault operation using model-based predictive current control techniques," *IEEE Trans. Ind. Electron.*, vol. 61, no. 9, pp. 4474–4484, Sep. 2014.
[22] E. Fuentes, D. Kalise, J. Rodriguez, and R. Kennel, "Cascade-free predictive speed control for electric drives," *IEEE Trans. Ind. Electron.*, vol. 61, no. 5, pp. 2176–2184, May 2014.
[23] M. Habibullah and D. D.-C. Lu, "A speed-sensorless FS-PTC of induction motors using extended Kalman filters," *IEEE Trans. Ind. Electron.*, vol. 62, no. 11, pp. 6765–6778, Nov. 2015.
[24] P. Vaclavek and P. Blaha, "Field weakening implementation in AC induction machine predictive control," in *Proc. IEEE 9th Int. Conf. Power Electron. Drive Syst. (PEDS)*, Singapore, 2011, pp. 171–176.
[25] S. Mariéthoz, A. Domahidi, and M. Morari, "High dynamic performance constrained optimal control of induction motors," in *Proc. 25th Annu. IEEE Appl. Power Electron. Conf. Expo. (APEC)*, Palm Springs, CA, USA, 2010, pp. 1995–2001.
[26] S. Mariéthoz, A. Domahidi, and M. Morari, "High-bandwidth explicit model predictive control of electrical drives," *IEEE Trans. Ind. Appl.*, vol. 48, no. 6, pp. 1980–1992, Nov./Dec. 2012.
[27] C. V. Rao, S. J. Wright, and J. B. Rawlings, "Application of interior-point methods to model predictive control," *J. Optim. Theor. Appl.*, vol. 99, no. 3, pp. 723–757, Dec. 1998.
[28] M. H. Wright, "The interior-point method revolution in optimization: History, recent developments, and lasting consequences," *Amer. Math. Soc.*, vol. 42, no. 1, pp. 39–56, Sep. 2004.
[29] M. S. K. Lau, S. P. Yue, K. V. Ling, and J. M. Maciejowski, "A comparison of interior point and active set methods for FPGA implementation of model predictive control," in *Proc. Eur. Control Conf. (ECC)*, Budapest, Hungary, 2009, pp. 156–161.
[30] J. Nocedal and S. J. Wright, *Numerical Optimization*. New York, NY, USA: Springer, 1999.
[31] R. Fletcher, *Practical Methods of Optimization*, 2nd. ed. Hoboken, NJ, USA: Wiley, May 2000.
[32] S. Boyd and L. Vandenberghe, *Convex Optimization*. Cambridge, U.K.: Cambridge Univ. Press, 2009.
[33] H. J. Ferreau, H. G. Bock, and M. Diehl, "An online active set strategy to overcome the limitations of explicit MPC," *Int. J. Robust Nonlinear*, vol. 18, no. 8, pp. 816–830, May 2008.
[34] Y. Wang and S. Boyd, "Fast model predictive control using online optimization," *IEEE Trans. Control Syst. Technol.*, vol. 18, no. 2, pp. 267–278, Mar. 2010.
[35] A. K. Abbes, F. Bouani, and M. Ksouri, "A microcontroller implementation of constrained model predictive control," *World Acad. Sci. Eng. Technol.*, vol. 5, no. 8, pp. 655–662, Aug. 2011.
[36] A. Wills, A. Mills, and B. Ninness, "FPGA implementation of an interior-point solution for linear model predictive control," in *Proc. 24th Int. Conf. Field Program. Logic Appl. (IFAC)*, Milan, Italy, 2011, pp. 14527–14532.
[37] A. Bemporad, M. Morari, V. Dua, and E. N. Pistikopoulos, "The explicit linear quadratic regulator for constrained systems," *Automatica*, vol. 38, no. 1, pp. 3–20, Jan. 2002.
[38] P. Grieder, M. Kvasnica, M. Baotić, and M. Morari, "Low complexity control of piecewise affine systems with stability guarantee," in *Proc. Amer. Control. Conf. (ACC)*, Boston, MA, USA, 2004, pp. 1196–1201.
[39] A. Bemporad and C. Filippi, "Suboptimal explicit receding horizon control via approximate multiparametric quadratic programming," *J. Optim. Theory Appl.*, vol. 117, no. 1, pp. 9–38, Apr. 2003.
[40] A. Alessio and A. Bemporad, "A survey on explicit model predictive control," in *Nonlinear Model Predictive Control*. New York, NY, USA: Springer, 2009, pp. 345–369.
[41] J. Löfberg, "YALMIP: A toolbox for modeling and optimization in MATLAB," in *Proc. Int. Symp. Comput. Aided Control Syst. Design (CACSD)*, Taipei, Taiwan, 2004, pp. 284–289.
[42] M. Kvasnica, P. Grieder, M. Baotić, and M. Morari, "Multi-parametric toolbox (MPT)," in *Proc. Hybrid Syst. Comput. Control (HSCC)*, Philadelphia, PA, USA, 2004, pp. 448–462.
[43] Z. Hu and K. Hameyer, "Robust predictive current control for performance improvement of induction motors with parameter variation," in *Proc. 41st Annu. Conf. IEEE Ind. Electron. Soc. (IECON)*, Yokohama, China, 2015, pp. 451–456.

Zheng Hu received the diploma in computer science in 2008 and the diploma in industrial engineering in 2011 from RWTH Aachen University, Aachen, Germany.

Until January 2012, he was with Gesellschaft für Industrieforschung mbH, Alsdorf, Germany, as a Software Engineer, working in the field of automatic transmission controls. He is currently a Research Associate with the Institute of Electrical Machines, RWTH Aachen University, where he focuses his work on optimal control of electric drive systems.

Kay Hameyer (M'96–SM'99) received the diploma in electrical engineering from the University of Hanover, Hanover, Germany, and the Ph.D. degree from the Berlin University of Technology, Berlin, Germany, in 1992.

In 1996, he became a Full Professor of Numerical Field Computations and Electrical Machines, KU Leuven, Leuven, Belgium. Since 2004, he has been a Full Professor and the Director of the Institute of Electrical Machines, RWTH Aachen University, Aachen, Germany. In 2006, he was a Vice Dean of the faculty and, from 2007 to 2009, he was the Dean of the Faculty of Electrical Engineering and Information Technology, RWTH Aachen University. His work is concerned with the development of magnetic levitation for drive systems, magnetically excited audible noise in electrical machines, and the characterization of ferro-magnetic materials. He has authored/coauthored more than 250 journal publications, more than 500 international conference proceedings papers, and is the author of four books. His research interests include numerical field computation and optimization, the design and controls of electrical machines, in particular, permanent-magnet excited machines, induction machines, and design employing the methodology of virtual reality.

Dr. Hameyer is a member of the VDE and a Fellow of the Institution of Engineering and Technology, U.K.